Research Article | Vol. 26, No. 13 | 25 Jun 2018 | OPTICS EXPRESS 16609
Optics EXPRESS

Calibration sample for arbitrary metrological characteristics of optical topography measuring instruments

MATTHIAS EIFLER,[1,*] JULIAN HERING,[2] GEORG VON FREYMANN,[2,3] AND JÖRG SEEWIG[1]

[1]*Institute for Measurement and Sensor Technology, University of Kaiserslautern, Gottlieb Daimler Straße 44, 67663 Kaiserslautern, Germany*
[2]*Physics Department and Research Center OPTIMAS, University of Kaiserslautern, Erwin-Schrödinger-Str. 56, 67663 Kaiserslautern, Germany*
[3]*Fraunhofer Institute for Industrial Mathematics ITWM, Fraunhofer Platz 1, 67663 Kaiserslautern, Germany*
[*]*meifler@mv.uni-kl.de*

Abstract: Areal optical surface topography measurement is an emerging technology for industrial quality control. However, neither calibration procedures nor the utilization of material measures are standardized. State of the art is the calibration of a set of metrological characteristics with multiple calibration samples (material measures). Here, we propose a new calibration sample (artefact) capable of providing the entire set of relevant metrological characteristics within only one single sample. Our calibration artefact features multiple material measures and is manufactured with two-photon laser lithography (direct laser writing, DLW). This enables a holistic calibration of areal topography measuring instruments with only one series of measurements and without changing the sample.

OCIS codes: (120.6660) Surface measurements, roughness; (150.1488) Calibration; (110.6895) Three-dimensional lithography; (180.6900) Three-dimensional microscopy.

References and links

1. R. Leach, *Characterisation of areal surface texture* (Springer, 2013). Chap. 1.
2. K. Stout, *Development of methods for the characterisation of roughness in three dimensions* (Penton, 2000).
3. L. Blunt and X. Jiang, *Advanced techniques for assessment surface topography: Development of a basis for 3D surface texture standards SURFSTAND* (Kogan Page Science, 2003).
4. J. Seewig and M. Eifler, "Calibration of areal surface topography measuring instruments," Proc. SPIE **10449**, 1044911 (2017).
5. International Organization for Standardization, "Geometrical product specifications (GPS) - Surface texture: Areal - Part 1: Indication of surface texture," ISO 25178–1 (2016).
6. International Organization for Standardization, "Geometrical product specifications (GPS) - Surface texture: Areal - Part 601: Nominal characteristics of contact (stylus) instruments," ISO 25178–601 (2010).
7. International Organization for Standardization, "Geometrical product specifications (GPS) - Surface texture: Areal - Part 600: Metrological characteristics for areal-topography measuring methods," ISO/DIS 25178–600 (2018).
8. International Organization for Standardization, "Geometrical product specifications (GPS) - Surface texture: Areal - Part 701: Calibration and measurement standards for contact (stylus) instruments," ISO 25178–701 (2010).
9. International Organization for Standardization, "Geometrical product specifications (GPS) - Surface texture: Areal - Part 700: Calibration and verification of areal topography measuring instruments," ISO 25178–700.3:2016, WD (2016).
10. C. L. Giusca, R. K. Leach, F. Helary, T. Gutauskas, and L. Nimishakavi, "Calibration of the scales of areal surface topography-measuring instruments: part 1. Measurement noise and residual flatness," Meas. Sci. Technol. **23**(3), 035008 (2012).
11. C. L. Giusca, R. K. Leach, and F. Helery, "Calibration of the scales of areal surface topography measuring instruments: part 2. Amplification, linearity and squareness," Meas. Sci. Technol. **23**(6), 065005 (2012).
12. C. L. Giusca and R. K. Leach, "Calibration of the scales of areal surface topography measuring instruments: part 3. Resolution," Meas. Sci. Technol. **24**(10), 105010 (2013).

#323218 https://doi.org/10.1364/OE.26.016609
Journal © 2018 Received 13 Feb 2018; revised 17 May 2018; accepted 21 May 2018; published 14 Jun 2018

Optics EXPRESS

13. R.K. Leach, C.L. Giusca, and P. Rubert, "A single set of material measures for the calibration of areal surface topography measuring instruments: the NPL Areal Bento Box," in Proceedings of Met and Props, 406–413 (2013).
14. R. K. Leach, C. L. Giusca, K. Rickens, O. Riemer, and P. Rubert, "Development of material measures for performance verifying surface topography measuring instruments," Surf. Topo. Met.Prop. **2**(2), 025002 (2014).
15. P. de Groot, "Progress in the specification of optical instruments for the measurement of surface form and texture," Proc. SPIE **9110**, 91100M (2014).
16. P. de Groot, "The Meaning and Measure of Vertical Resolution in Optical Surface Topography Measurement," Appl. Sci. **7**(1), 54 (2017).
17. J. K. Hohmann, M. Renner, E. H. Waller, and G. von Freymann, "Three-Dimensional μ-Printing: An Enabling Technology," Adv. Optical Mater. **3**(11), 1488–1507 (2015).
18. M. Eifler, J. Seewig, J. Hering, and G. von Freymann, "Calibration of z-axis linearity for arbitrary optical topography measuring instruments," Proc. SPIE **9525**, 952510 (2015).
19. F. Ströer, J. Hering, M. Eifler, I. Raid, G. von Freymann, and J. Seewig, "Ultrafast 3D High Precision Print of Micro Structures for Optical Instrument Calibration Procedures," Additive Manufacturing **18**, 22–30 (2017).
20. M. Eifler, J. Hering, G. von Freymann, and J. Seewig, "Manufacturing of the ISO 25178-70 material measures with direct laser writing – a feasibility study," Surf. Topo. Met.Prop. in press.
21. G. V. Samsonov, *Handbook of the Physicochemical Properties of the Elements* (Springer, 1968).
22. R. Krüger-Sehm, P. Bakucz, L. Jung, and H. Wilhelms, "Chirp-Kalibriernormale für Oberflächenmessgeräte (Chirp Calibration Standards for Surface Measuring Instruments)," Techn. Mess. **74**(11), 572–576 (2007).
23. J. Seewig, M. Eifler, and G. Wiora, "Unambiguous evaluation of a chirp measurement standard," Surf. Topo. Met.Prop. **2**(4), 045003 (2014).
24. International Organization for Standardization, "Geometrical product specifications (GPS) – Surface texture: Areal – Part 603: Nominal characteristics of non-contact (phase-shifting interferometric microscopy) instruments," ISO 25178–603 (2013).
25. International Organization for Standardization, "Geometrical product specifications (GPS) – Surface texture: Areal – Part 2: Terms, definitions and surface texture parameters," ISO 25178–2 (2012).
26. International Organization for Standardization, "Geometrical product specification (GPS) – Surface texture: Areal – Part 70: Material measures," ISO 25178–70 (2014).
27. M. Eifler, "Modellbasierte Entwicklung von Kalibriernormalen zur geometrischen Produktspezifikation," Kaiserslautern: Technische Universität Kaiserslautern (2016).
28. Deutsches Institut für Normung, "Terms and definitions used on ageing of materials – Polymeric materials," DIN 50035 (2012).
29. K. Klauer, M. Eifler, F. Schneider, J. Seewig, and J. C. Aurich, "Ageing of roughness artefacts – impact on the measurement results," in Proceedings of euspen's Int. Conf. & Exhibition **17**, 403–404 (2017).
30. D. W. Hoffman and J. A. Thornton, "Internal stresses in sputtered chromium," Thin Solid Films **40**, 355–363 (1977).
31. J. S. Oakdale, J. Ye, W. L. Smith, and J. Biener, "Post-print UV curing method for improving the mechanical properties of prototypes derived from two-photon lithography," Opt. Express **24**(24), 27077–27086 (2016).

1. Introduction

In the past decades, areal surface topography measurement has emerged (see e.g [1–3]. for a historical overview). Based on the increasing industrial application, the WG 16 "Areal and profile surface texture" of the ISO Technical Committee 213 started to work on the standard ISO 25178 "Geometrical product specifications (GPS) - Surface texture: Areal" in 2003 [4,5]. For the calibration of areal surface topography measuring instruments, the ISO 25178-6xx series (see e.g [6].) defines the metrological characteristics: part 600 in a general way and the other parts for specific measuring principles.

A metrological characteristic is defined as a characteristic "which may influence the results of a measurement" [7] and thus, should be considered during the measuring process. The ISO 25178-600 therefore defines currently the following basic metrological properties for a surface topography measurement [7]: (i) the amplification coefficient of the three axes describes the slope of the response function of the axis. (ii) The linearity deviation of an axis is the maximum local difference between the straight-line fit of the response function and the measured response function itself. (iii) The flatness deviation, which is the maximum deviation between an ideal plane and its measured topography. (iv) The measurement noise and (v) the topographic spatial resolution are characteristics of the height axis. (vi) The x-y mapping deviation describes the local deviations of the lateral axes including their perpendicularity. (vii) The topography fidelity characterizes whether the measuring instrument adequately transfers topographic features.

Optics EXPRESS

As the metrological characteristics can be determined by performing measurement tasks, they are subject to the calibration of topography measuring instruments, which is described in the ISO 25178-7xx series (see e.g [8].). The structure is identical to the 6xx series: part 700 [9] gives a basic framework for general calibration procedures whereas the other parts define calibration tasks which are specific for a certain measuring principle. The calibration tasks are performed with material measures (also known as measurement standards or calibration artefacts) that feature defined metrological characteristics. State of the art is the calibration of metrological characteristics with multiple material measures and samples. A practical approach for the determination of all general metrological characteristics has been introduced by Giusca et al. [10–12]. In order to perform a cost- and time-efficient calibration of all characteristics, it is essential to use as few as possible material measures that feature and calibrate all relevant metrological characteristics reliably. A set of five single material measures for measuring all metrological characteristics has been introduced with the NPL BentoBox [13] in 2013 which also includes material measures for the calibration of the measurement of areal surface texture parameters [14]. Additionally, the practical specification of topography measuring instruments based on the metrological characteristics is subject to research work and aims at achieving acceptance of the new definitions within the industrial application [15,16].

Until now, however, a set of multiple material measures is still necessary for a holistic calibration of the metrological characteristics and thus, a high amount of work is required for an instrument calibration. An easier calibration procedure and less measuring effort are required if only one sample featuring all metrological characteristics could be used. In the following, we propose an approach which allows the calibration of arbitrary metrological characteristics with only one sample featuring several material measures. We use direct laser writing (DLW) to fabricate the according samples [17]. The general suitability of DLW for the manufacturing of calibration geometries has already been proven in previous studies [18–20].

2. Sample fabrication

DLW offers the possibility of fabricating almost arbitrary 3D structures: an acrylate-based negative-tone photo resist (IP-S, *Nanoscribe GmbH*) is scanned by the focus of a femtosecond pulsed laser beam (λ = 780 nm, 63x objective, NA = 1.4). Following to two-photon absorption, the polymerization takes only place within the very focal volume, allowing for the generation of true 3D structures. We fabricate all samples with a Photonic Professional GT (*Nanoscribe GmbH*). According to the technical specification of this device, the lateral resolution and minimal feature size are 500 nm and 200 nm, respectively, while ensuring a very high fabrication velocity (>10000 µm/s). Thus, the device fulfills all necessary requirements of a fast and highly precise fabrication of various (surface) structures. In order to be applicable for the manufacturing of material measures, the fabrication process needs to be at least as precise as the measuring instruments to be calibrated. We realize all desired sample geometries with Matlab and export the sample files to a stereo lithography format (.stl) (see section 3). Subsequently, those files are separated horizontally (hatching) and vertically (slicing) to x, y and z coordinates for the deflection of the laser focus. For all geometries, those parameters, as well as scan speed and excitation power are optimized iteratively controlling the outcome with a light microscope (Olympus BX60, *Olympus K.K.*).

As we use the samples for the calibration of optical topography measuring instruments, they must feature reflective surface properties. Because metallic materials can currently not be directly fabricated with DLW, we coat the surface after manufacturing. As standard coating material in optics, gold (Au) is chosen and sputtered with a layer thickness of 20 nm. Due to the weak bonding between the (glass-) substrate and the gold-layer, a thin (10 nm) chromium-layer (Cr) is required as an adhesion-promoting agent and thus, chromium itself is analyzed as a second coating material as well. Generally, the samples should be mechanically

Optics EXPRESS

stable to allow for a tactile sampling. Hence, iridium (Ir) is chosen as another coating material, as it possesses a high Vickers hardness (see [21]).

Regarding the calibration procedure of low magnification objectives (e.g. 5x), some of the desired measures have to be on a scale of almost 1 mm^2. Since the scanning field of the DLW system is limited to approximately 300 µm x 300 µm, those large geometries are stitched together. Here, single fields of smaller dimension (max. 120 µm x 120 µm) are chosen to minimize the influence of vignetting. The positioning accuracy of the stage is approximately 1 µm. Thus, for the elimination of possible stitching gaps, a 2 µm overlap of the separated fields is applied.

In the end, the fabrication time of all geometries necessary for a complete calibration procedure of an optical measuring device using the most common objectives (5x, 10x, 20x, 50x, 60x and 100x magnification) and, thus, the fabrication time of this "universal calibration artefact" sums up to less than 10 hours and can be realized easily overnight.

3. Design of a "universal calibration artefact" and calibration strategies

For the calibration of optical 3D topography measuring instruments, the basic metrological characteristics as introduced in section 1 are taken into account. Figure 1(a) visualizes the simulated manufacturing data of the required six target geometries. Depending on the microscopic magnification, the objective's field of view determines the required size of the structure. 100 µm x 100 µm, 200 µm x 200 µm, 400 µm x 400 µm and 800 µm x 800 µm samples are considered in order to provide typical sample sizes for 100x, 60x, 50x, 20x, 10x and 5x magnifications.

As pre-processing algorithm, the inner 80% of each measured structure are extracted, aligned and the parameters defined within the ISO 25178-2 and −70 [25,26] are calculated. Afterwards, the individual parameters of each geometry are examined. For a holistic calibration, the following material measures and evaluation routines are required.

The Siemens Star geometry (type ASG [26]) may be used to obtain a width metric related to the topographic spatial resolution as described in ISO 25178-600 (W_R) [12]. This parameter is indicated with the term "ASG width metric". For the target data set 16 petals featuring a height of 1 µm are chosen. The lateral resolution limit of the measuring instrument is determined as described by Giusca and Leach [12]. Furthermore, the surface texture parameters S_a and S_q are evaluated in order to additionally characterize the height axis of the examined measuring device.

For the measurement of the topography fidelity T_{FI}, a chirp-standard (type CIN [22]) is used as suggested by Seewig et al. who introduced an according evaluation and calibration routine [23]. However, currently there is not yet an agreement on the standardization of the fidelity calibration and the determination of according parameters. The chirped sample features sinusoidal profiles with an amplitude of 3 µm and 20 different wavelengths between 9.46 µm and 0.47 µm (considering the 100 µm x 100 µm sample). The sample is as well characterized by S_a and S_q. Additionally, the small scale fidelity limit ssf [23] is calculated, corresponding to a transmission of the target amplitude of ± 50%.

A flatness standard (type AFL [26]) allows for the calibration of the noise N_M and the residual flatness z_{FLT} of the height axis [10]. Here, S_a and S_q can be applied to evaluate the metrological characteristics as they are directly correlated with noise and flatness.

Using a radial sinus wave (type ARS [26]), an integral calibration of the measuring device with a period length of 10 µm (considering again the 100 µm x 100 µm sample) and an amplitude of 3 µm is possible. The integral transfer characteristics of the measuring device are evaluated with S_a and S_q as described in ISO 25178-70 [26].

Optics EXPRESS

For the lateral axes, a cross-grating (type ACG [26]) allows for the calibration of the *x*- and *y*-axis mapping deviation by a determination of the linearity l_x, l_y, amplification coefficients α_x, α_y and the perpendicularity Δ_{PERxy} of the axes as suggested by Giusca et al. [11]. In doing so, the entire calibration of the lateral axes is possible with the aid of one calibration geometry. A pitch length of 10 µm (considering again the 100 µm x 100 µm sample), an amplitude of 3 µm and a groove width of 6 µm are chosen. The pitch lengths of the grating in both lateral directions and the angle β between the gratings in *x*- und *y*-direction are evaluated for the determination of the described characteristics.

Considering the calibration of the height axis we apply a modification of the current ISO 25178-60x series. For example, in the ISO 25178-603 [24], which describes the metrological characteristics for phase-shifting interferometers, the determination of the linearity l_z and the amplification coefficient α_z of the height axis is suggested based on the response function of the axis [24]. Usually, this response function is estimated by measuring various step height artefacts [11]. Instead we chose an irregular roughness calibration geometry (type AIR [26]) with a deterministic structure and a linear Abbott-curve as according material measure. Previously, we showed that this allows for a similar calibration of the linearity l_z and the amplification coefficient α_z of the height axis [18,27]. Additionally, an integral calibration of the device based on the 3D roughness parameters is possible with the type AIR geometry [18]. The surface topography is based on an actual engineering surface and thus enables a practical calibration of multiple properties of surface topography measuring instruments. The aforementioned linear Abbott-curve allows to achieve an almost stepless calibration of the height axis [18,27]. Additionally to specific linearity criteria that compare the $n \cdot m$ topography heights of the measured Abbott-curve $C(Mr)$ with the target Abbott-curve, we use an alternative analysis to derive α_z and l_z, the parameters described in the ISO 25178-60x series [24]. In doing so, the response function of the axis is not determined with a series of step height measurements but with all height values of the Abbott-curve of the proposed type AIR material measure:

$$\left(C\left(Mr_k\right), C_{tar}\left(Mr_k\right)\right),\ k = 1, \ldots, n \cdot m, \tag{1}$$

where $C(Mr)$ represents the function of the measured Abbott-curve and $C_{tar}(Mr_k)$ of the virtual sample [27]. In order to neglect possible outliers, the straight line fit of the transmission is performed with the inner 80% of the height values and leads to a least squares fit with the slope m and the intercept t [27]. These parameters are used to determine the ISO criteria of amplification coefficient and linearity deviation [24,27]:

$$l_z = \max\left(\left|C\left(Mr_k\right) - \left(m \cdot C_{tar}\left(Mr_k\right) + t\right)\right|\right),\ k = 1, \ldots n \cdot m,\ \alpha_z = m. \tag{2}$$

The fit of the slope equals the measured amplification coefficient, whereas the largest pointwise deviation between the fit and the original data set of the response function is the linearity deviation as defined within for example the ISO 25178-603 [24]. The proposed method uses a large number of topography points for a determination of the *z*-axis linearity instead of only using a small number of step heights for the response function estimation. Additionally to the parameters based on the response function, S_a and S_q of the sample can be evaluated for the integral calibration [18,27].

The resulting “universal calibration artefact” is shown in Fig. 1(b). There, a scanning electron microscopic (SEM) image of one type ARS sample is shown exemplarily. DLW allows for fabricating all of the aforementioned geometries on one single sample. Thus, a holistic calibration is possible without changing and adjusting the sample several times. Even for varying microscopic magnifications only one sample is required: the geometries are

Optics EXPRESS

defined in a way that scaling under consideration of those different microscopic magnifications is possible. Therefore, the coordinates of the lateral axes are scaled with the factors two, four, and eight to additionally realize material measures with sizes of 200 µm x 200 µm, 400 µm x 400 µm and 800 µm x 800 µm on the same sample. The amplitudes of the different material measures are not changed by the scaling. Table 1 (Appendix) provides the evaluation parameters of the different geometries for their use with different fields of view and magnifications. Generally, due to the high versatility of the manufacturing, it is possible to perform almost any scaling of the proposed geometries in order to adapt the sample towards a specific measuring principle or instrument.

Subsequently, we examine the aging and scaling of these varying geometries in order to qualify the manufactured samples for practical calibration applications.

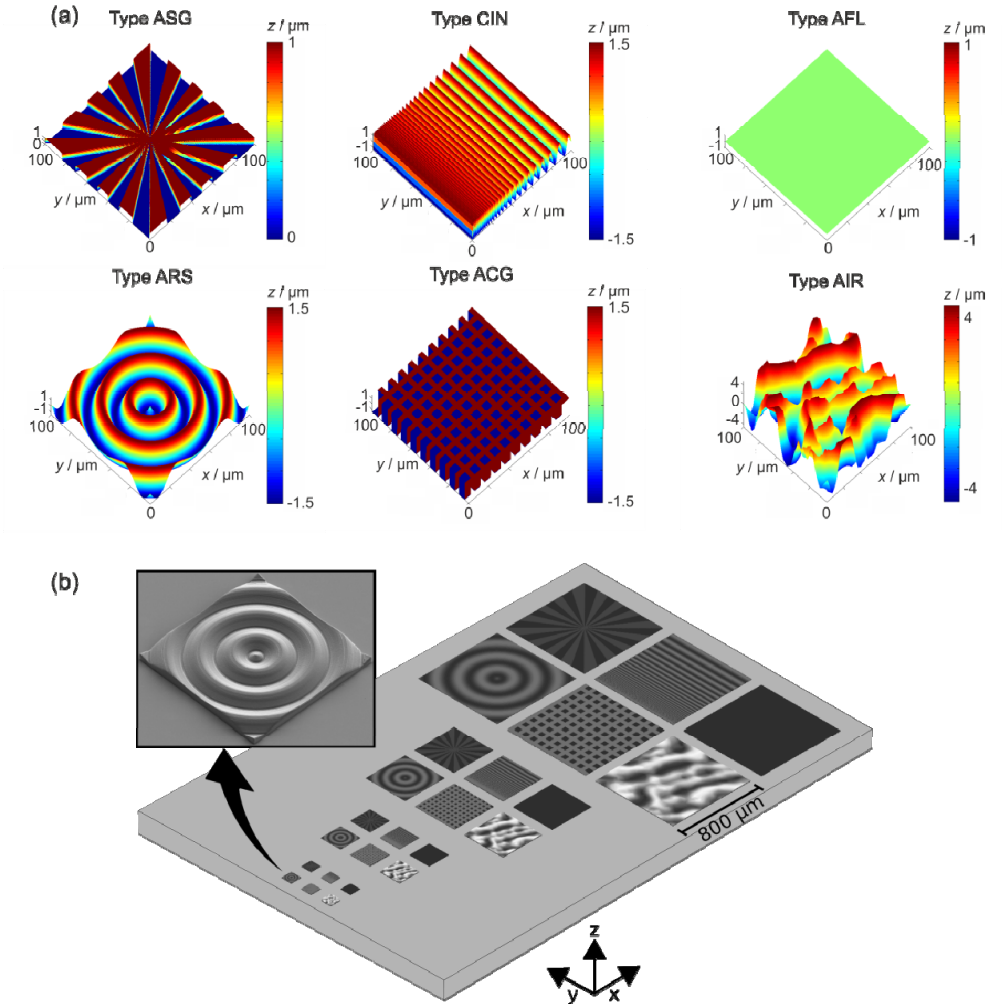

Fig. 1. (a) Target geometries imaged with a size of 100 µm x 100 µm (simulated data), (b) overview of all target geometries featuring varying sizes – the final "universal calibration artefact" (simulated data and SEM image of the type ARS material measure).

4. Aging study

In order to determine the time-dependent stability and the aging behavior of the manufactured samples, we perform an artificial aging study. Three identical samples, as illustrated in Fig. 1, are manufactured and a 30 nm metal coating is sputtered on top of the polymeric surface in

Optics EXPRESS

order to achieve suitable optical properties for surface topography measuring instruments. As described, Au, Cr (Univex 450C, *Oerlikon GmbH* for both) and Ir (Leica EM ACE600, *Leica Microsystems CMS GmbH*) are used in order to compare the varying coating materials and their respective aging behavior. Since aging is a time-dependent process [28], a climate chamber is used to emulate an accelerated artificial aging of the samples. In previous studies with material measures, which were manufactured with the aid of ultra-precision cutting, it has been shown that this examination method is suitable for the description of aging effects [29]. Therefore, this approach is used to investigate these effects for the direct laser written geometries as well.

First, we take a reference measurement of the structures with a size of 100 µm x 100 µm. Then, the samples are stored at 80°C within the climate chamber and additional measurements after t = 1, 2, 5, 8, 12 and 19 days storage time are performed. Here, dry air conditions are realized with the aid of a drying agent. For each measurement, the described evaluation parameters are examined and their time-dependent behavior is investigated. Sample measurements are taken with a confocal microscope NanoFocus µSurf with 100x magnification. The instrument is linked to a traceability chain based on other certified material measures.

Figure 2 summarizes the results of the chirped standard (type CIN) exemplarily: the evaluation parameters S_a and S_q of the coatings gold, chromium and iridium are compared to their respective target values shown in Table 1. Additionally, the absolute values of the *small scale fidelity* are provided. It can be observed that the measurement results of both lateral resolution parameters, the *small scale fidelity limit* determined by the chirped standard and the ASG width metric determined by the Siemens Star (Appendix) are influenced by the aging process. The aged surfaces enable a measurement of narrower areas of the petals or the sinusoidal structures, respectively. This is as well corroborated by the roughness parameters S_a and S_q who tend to decrease during the first few days.

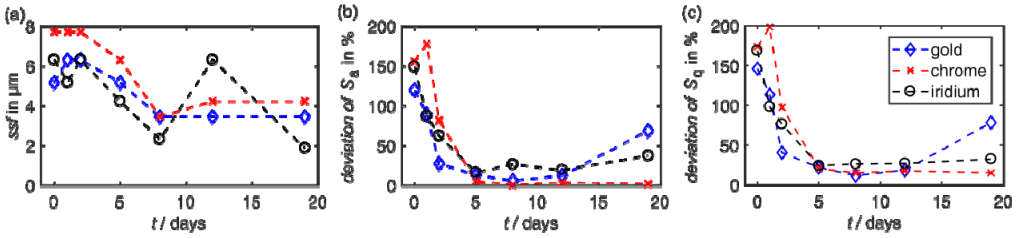

Fig. 2. Aging study exemplarily shown for the type CIN material measure. Evaluated parameters: (a) *small scale fidelity limit* (*ssf*) as defined in [23], (b) deviation of arithmetic mean roughness (S_a-$S_{a,tar}$) / $S_{a,tar}$ and (c) deviation of root mean square roughness (S_q-$S_{q,tar}$) / $S_{q,tar}$.

All parameters stabilize after a certain amount of time and thus indicate a stationary aging result. This effect is more significant for the chirp standard as more areas with narrow structures and steep angles are present (see Fig. 2). When the varying coatings are compared, equal results are achieved. However, the Au-coating does not provide as stable roughness parameters as the other materials for the chirped standard.

The significant change of the parameter values can be additionally explained when profiles are extracted from the measured data sets after different aging times, e.g. for the sample with Iridium-coating. This is shown in Fig. 3. There, an extracted profile which was used for the chirp evaluation is displayed before the aging commences (t = 0 days) and after storage times of t = 5, 8 and 19 days in the climate chamber. The large deviations at the beginning of the amplitude roughness parameters can be explained as follows: due to sharp edges there are many optical artefacts before the aging which lead to an increased measured roughness. During the aging process, the sharp edges are smoothed and the structures become

Optics EXPRESS

optically more cooperative for the measurement. In consequence, the massive change in the roughness parameters is not only caused by the shrinking itself but much stronger by the reducing number of optical artefacts.

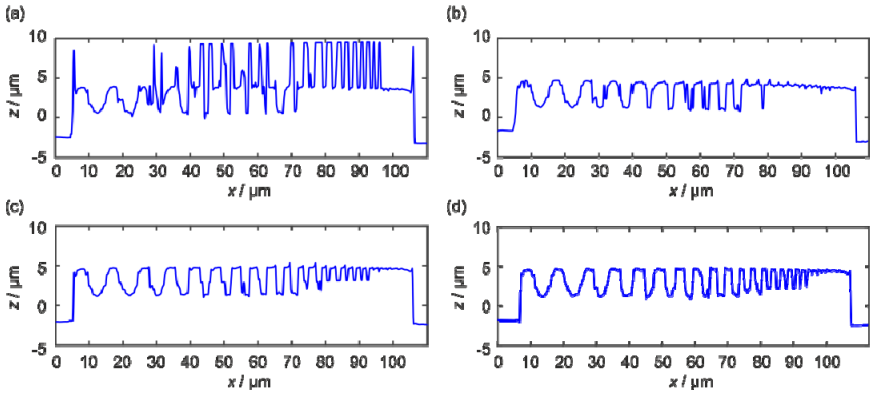

Fig. 3. Aging study, exemplary profiles for the Ir-coated type CIN material measure. (a) Extracted profile before aging (t = 0 days), (b) extracted profile after t = 5 days of aging, (c) extracted profile after t = 8 days of aging, (d) extracted profile after t = 19 days of aging.

An exemplified evaluation of the *small scale fidelity limit* is illustrated in Fig. 4. There, the extracted profile from the geometry with the Ir-coating after a storage time of t = 19 days is shown, as well as its evaluation with the application of the *ssf*. In Fig. 4(a), the fit of the nominal sinusoidal surface structures of the chirp-geometry is illustrated, whereas Fig. 4(b) shows the determination of the *ssf* based on these fits: the fitted amplitudes are imaged for the different estimated period lengths of the fit. The *ssf* can be determined as smallest period length where the amplitude of the fit deviates less than 50% from the target amplitude [23]. In the given example, this limit is determined to a period length of 1.91 µm which is estimated to 1.86 µm. Thus, it can be concluded that both, the laser lithographic manufacturing and the measuring process maintain a small scale fidelity up to the micrometer-scale. It cannot be distinguished whether the manufacturing or the measuring is the limiting process here. This can be clarified with further studies using high-resolution AFM measurements.

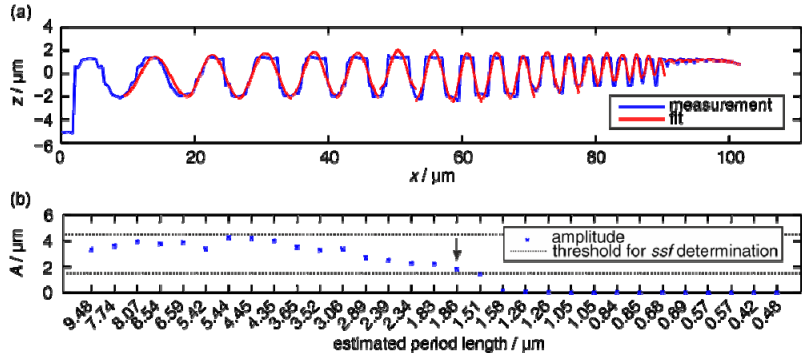

Fig. 4. Aging study based on the *small scale fidelity limit*, exemplarily shown for the Ir-coated type CIN material measure after t = 19 days. (a) Fit (red) of the measured (blue) chirp geometry, (b) *small scale fidelity limit* (*ssf*) determination.

Examining the other ISO-based geometries, the given observations are well confirmed. All results are given in the Appendix (Figs. 10, 11, 12, and 13). The roughness values of the flat surface (type AFL) decrease with increasing time as the structure is also smoothed through shrinking or warping effects. The parameters of the radial sinus wave (type ARS) do not change significantly as the structure exhibits only small angles and is thus not heavily

Optics EXPRESS

influenced by the changes. This is in contrast to the chirp structure, which exhibits large areas with narrow structures. The observations of Fig. 3 support the explanation: the aging leads to significant changes in the areas with steep angles as they cause optical artefacts. After the aging occurs, the surface becomes more optically cooperative. When the cross-grating (type ACG) is evaluated, the lateral pitch lengths both in *x*- and *y*-direction do not change throughout the aging process as well as the perpendicularity between both axes. The parameters only scatter statistically. Thus, it can be concluded that mainly the height axis is influenced by the aging.

This effect is further examined with the type AIR material measure. The results of the evaluation are displayed in Fig. 5. Similar to the previous observations, the surface texture parameters decrease during the aging process. As in the rough surface many steep angles are present, the effect is significant. After a few days, also a stationary behavior is achieved and no more significant changes occur. This is also valid when the ISO 25178-60x parameters of the height axis, amplification coefficient and linearity deviation, are observed. The first one approaches the target value of 1 and the latter one decreases as well. The results are more or less independent from the coating material with a small offset only when the linearity deviation for the Cr-coating is examined. For the evaluation, we calculate these parameters as suggested in previous work [18,27] (see section 3): all height values of the measurement data are compared with the linear target Abbott-curve and the inner 80% of the height values serve for the response function estimation. This evaluation method leads to a high correlation of the amplification coefficient and the S_a -value. Figure 6 shows the resulting topographies and measured Abbott-curves before the aging (t = 0 days) and after t = 19 days storage time in the climate chamber for the sample with the Ir-coating. Again, the optical artefacts due to steep angles influence the measured metrological characteristics. This is also illustrated by the comparisons of the measured and the target Abbott-curve.

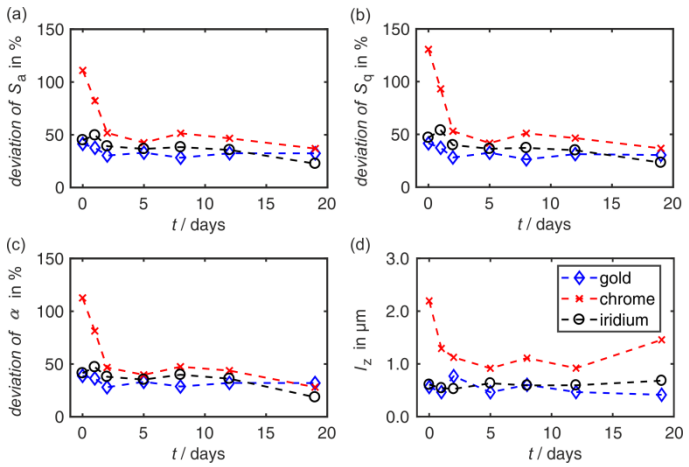

Fig. 5. Aging study. Evaluation of the parameters: (a) deviation of arithmetic mean roughness (S_a-$S_{a,tar}$) / $S_{a,tar}$, (b) deviation of root mean square roughness (S_q-$S_{q,tar}$) / $S_{q,tar}$, (c) deviation of the *amplification coefficient* α and (d) *linearity deviation* l_z as defined in ISO 25178-60x series for the type AIR material measure.

Analyzing the three coatings of the samples with a light microscope we observe that the gold-coating appears friable and the chromium-coating features fissures, especially for the larger geometries. Because of these effects, as well to assess an error of those parameters, an additional investigation is carried out for both materials.

In order to verify these results, two structures, CIN and ARS (100 µm x 100 µm, respectively) serve for the additional examination and are measured 12 times after every time-step of a second aging study. Based on the repetitive measurements it is also possible to

Optics EXPRESS

obtain information regarding the measurement uncertainty. For the determination of the areal roughness parameters, standard deviations are found to be in the nanometer-range. Besides, the results are in good agreement with the first study: the sample with many steep angles (type CIN) shows a decrease of the areal roughness parameters within the aging process whereas the sample with few steep angles (type ARS) does not exhibit any change of the roughness parameters. However, the roughness parameters of the chirped standards do not change as significantly as in the first study. When the new samples are examined with a light microscope, the aforementioned quality issues of the coatings can be observed as well: the chromium-coating features fissures especially for the larger samples and the gold-coating appears to be friable. Since chromium grows under high internal stresses during the sputtering process, subsequent shrinkage effects of the polymerized photo resist (which increase with an increasing polymerized area) presumably lead to those cracks when re-expanding under atmospheric conditions [30]. On the other hand, gold tends to show a microcrystalline growth which can be an explanation of the observed granularity.

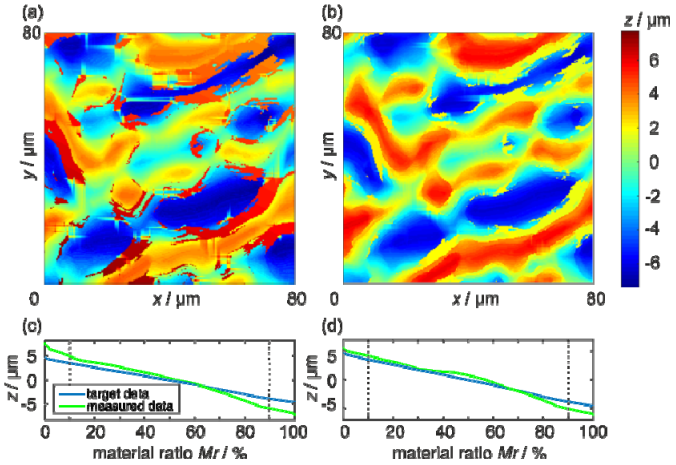

Fig. 6. Aging study. Evaluation of the type AIR geometry with Ir-coating: (a) measured topography before artificial aging (t = 0 days), (b) measured topography after t = 19 days, (c) measured Abbott-curve before artificial aging, (d) measured Abbott-curve after t = 19 days.

As the sample with the iridium-coating does feature a better quality and exhibits not only similar optical properties as gold but as well similar results in the aging study considering the examined parameters, this material is chosen for further examinations. Iridium is also the hardest material of the examined coatings and should therefore be suitable for a tactile sampling.

5. Scaling study

In order to perform a calibration of varying microscope magnifications, the structures are scaled to cover the different fields of view of typical optical surface topography measuring instruments. This scalability is characterized by measurements with the aforementioned confocal microscope using varying objectives. The structures feature sizes of 100 µm x 100 µm to 800 µm x 800 µm. Figure 7 illustrates exemplary the measured Ir-coated ARS material measure with 100x, 60x and 20x magnifications. It can be seen that a scaling of the geometry is generally possible. However, when the samples with edge lengths of 400 µm or larger are observed, stitching errors of the manufacturing process become visible which are caused by the described positioning accuracy of the stage (see section 2).

Additionally, the previously described roughness parameters can be evaluated in order to describe their scale-dependent effects. When the Siemens-Star (type ASG) is examined, it becomes observable that the ASG width measure is changing with the microscopic

Optics EXPRESS

magnification as the field of view and the sampling discretization change as well. The 100x and 60x objective magnifications feature a resolution of a few micrometers; the 20x magnification has a higher resolution limit. All results are displayed in the Appendix.

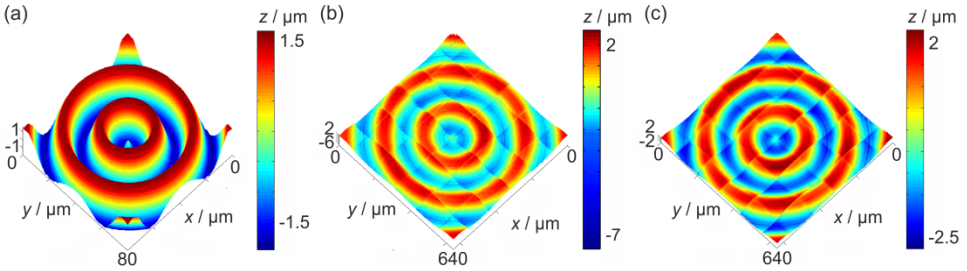

Fig. 7. Scaling study. Evaluation of the type ARS material measure with the above mentioned iridium coating. The 100 µm x 100 µm material measure is analyzed with a CM using (a) 100x magnification, whereas the 800 µm x 800 µm geometry is imaged using (b) 60x and (c) 20x magnification.

Figure 8 displays the results of the chirp standard (type CIN). The scaling of the chirp structure results in varying wavelengths of the sinusoidal structures. When the *small scale fidelity limit* is compared between the different measurements, it can be observed that larger samples lead to a bigger *small scale fidelity limit*. When the roughness parameters are compared, the 200 µm sample features the largest deviations. Since this sample is not stitched, vignetting obviously introduces stronger deviations than the following stitching errors. The 100 µm sample features the smallest deviations.

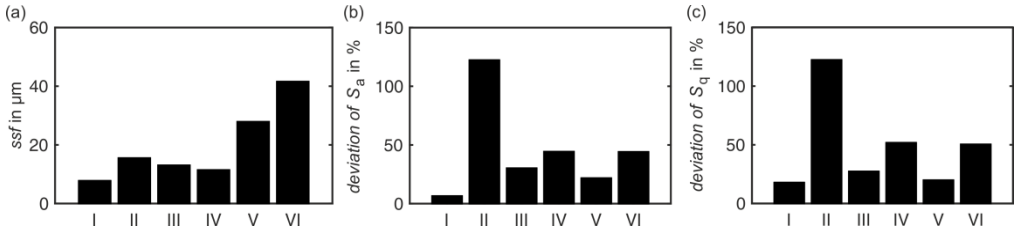

Fig. 8. Scaling study. Evaluation of the type CIN material measure. Evaluated parameters: (a) *small scale fidelity limit*, (b) deviation of arithmetic mean roughness (S_a-$S_{a,tar}$) / $S_{a,tar}$, (c) deviation of root mean square roughness (S_q-$S_{q,tar}$) / $S_{q,tar}$. I 100 µm sample measured with 100x magnification, II 200 µm sample, 60x magnification, III 400 µm sample, 20x magnification, IV 400 µm sample, 60x magnification, V 800 µm sample, 20x magnification, VI 800 µm sample, 60x magnification.

When the flat surface (type AFL) is examined (Appendix), the roughness values are very small for the 100 µm and 200 µm sample, whereas the larger material measures, which are stitched during the manufacturing process, show higher values of the roughness parameters. It can be observed that the stitching process in the manufacturing does have an influence on the averaged surface roughness (see also Fig. 7). As the objective of the AFL sample is to represent a perfectly smooth surface (with target values $S_a = S_q = 0$), the stitching effects are best visible here. Nevertheless, the areal sinusoidal material measure (type ARS) features very stable results, independent from scaling and objective magnifications (see Appendix). This is caused by the very smooth surface featuring no steep angles which cannot be transmitted by the measuring instrument. As the cross-grating (type ACG) is characterized by smooth surface structures and used for the lateral axes calibration, also here the target values of the different pitch lengths and perpendicularity are imaged properly independent from magnification and scaling of the sample.

The irregular roughness structure (type AIR) features steep surface angles and structures that are more complex. Thus, the scaling effects become more visible. Figure 9 shows the

Optics EXPRESS

results. It can be observed that an increased scaling of the geometry leads to a better compliance to the target values. The roughness values are smaller when larger structures are measured as the slope values decrease with an increasing scaling factor. Thus, the impact of the optical artefacts is significantly reduced when the larger structures are examined. This becomes as well visible when the linearity deviation and the amplification coefficient are compared as shown in Fig. 9(c) and 9(d). With a larger lateral scaling of the surface, the linearity deviation becomes significantly smaller and also the amplification coefficient tends towards its target value of 1. This indicates that the transmission characteristics improve with smaller surface slopes.

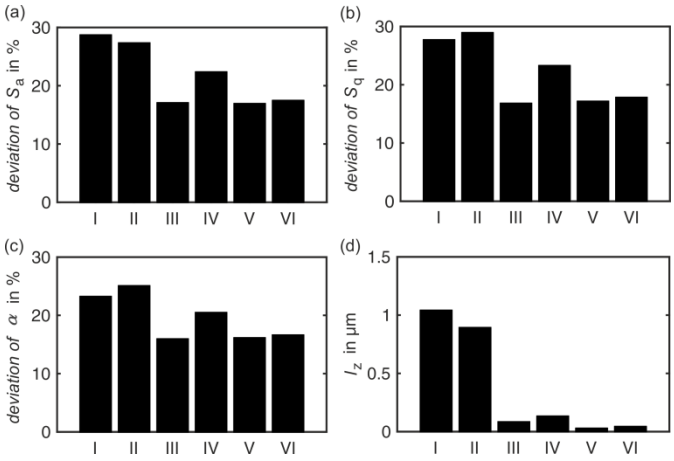

Fig. 9. Scaling study. Evaluation of the type AIR material measure. Evaluated parameters: (a) deviation of arithmetic mean roughness (S_a-$S_{a,tar}$) / $S_{a,tar}$, (b) deviation of root mean square roughness (S_q-$S_{q,tar}$) / $S_{q,tar}$, (c) deviation of the amplification coefficient α and (d) linearity deviation l_z as defined in the ISO 25178-60x series.

6. Summary and conclusion

The general manufacturing feasibility of material measures with DLW has been demonstrated in previous examinations. Here, a new sample was proposed that can calibrate all relevant metrological characteristics with just one set of measurements and one sample. This "universal calibration artefact" was examined regarding its practical abilities. In doing so, the aging behavior was investigated with different material coatings. It was shown that the structures as well as steep angles tend to smooth within the first days within a climate chamber. After that however, a stationary state is achieved. Thus, the sample is capable for practical application as aging improves the quality of the surface. As the iridium-coating showed the best surface quality, it was selected as the coating material for the following studies. For future work, it will be examined whether the aging process can be anticipated with a UV-postprocessing in order to achieve stable samples more quickly. In the study of Oakdale et al. [31] it was observed that the development of the polymer can be accelerated with this method.

A second criterion for the practical application, the scalability of the geometries, was as well examined. In doing so, it was shown that various microscopic magnifications can be calibrated with the proposed set of material measures when the lateral sizes of the structures are adapted towards the featured field of view. It was also shown that the samples with fewer steep angles that resulted from the scaling were easier to measure. However, larger structures which needed to be manufactured by stitching did show some differences, which e.g. had an influence towards the respective calibration properties of the smooth flat surface material measure. Other surfaces like the type AIR material measure featured smaller deviations with a larger scaling because the surface slopes decreased. For the quantitative characterization of

Optics EXPRESS

the actual stitching deviations just as well as for the determination of the lateral resolution of the manufacturing principle and its overall uncertainty, further measurements with an AFM will be conducted. With the confocal microscope however it was possible to perform an accurate characterization of the manufactured samples. In the end one can say that the proposed sample is useful for calibration of arbitrary metrological characteristics. With the proposed "universal calibration artefact" a time- and cost-efficient holistic calibration can be achieved as all metrological characteristics are imaged with one single sample.

Appendix

Table 1. Manufactured samples, target evaluation parameters.

structure type	structure size	100 µm x 100 µm	200 µm x 200 µm	400 µm x 400 µm	800 µm x 800 µm
ASG	S_a / µm	0.488	0.488	0.488	0.488
	S_q / µm	0.492	0.492	0.492	0.492
CIN	S_a / µm	0.960	0.960	0.960	0.960
	S_q / µm	1.065	1.065	1.065	1.065
AFL	S_a / µm	0.000	0.000	0.000	0.000
	S_q / µm	0.000	0.000	0.000	0.000
ARS	S_a / µm	0.944	0.944	0.944	0.944
	S_q / µm	1.053	1.053	1.053	1.053
ACG	l_x / µm	10	20	40	80
	l_y / µm	10	20	40	80
	α / °	90	90	90	90
AIR	S_a / µm	2.297	2.297	2.297	2.297
	S_q / µm	2.655	2.655	2.655	2.655

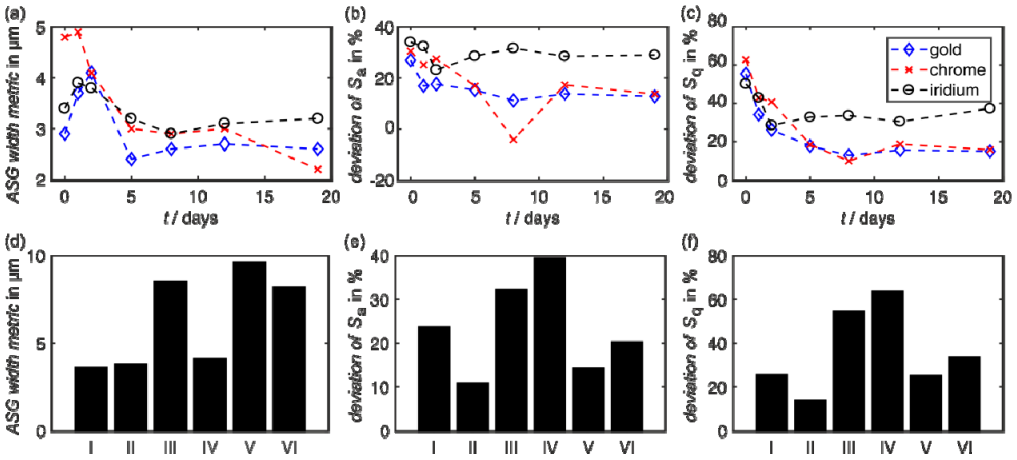

Fig. 10. Results of the type ASG material measure. (a)-(c): aging study; (d)-(f): scaling study. I-VI as described in Fig. 8.

Optics EXPRESS

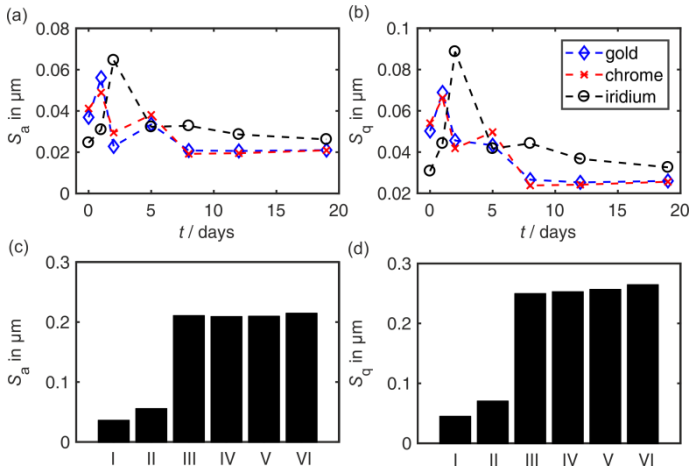

Fig. 11. Results of the type AFL material measure. (a)-(b): aging study; (c)-(d): scaling study. I-VI as described in Fig. 8. Because the target roughness parameters for the flat surface are $S_a = S_q = 0$, the measured parameters are plotted as absolute values.

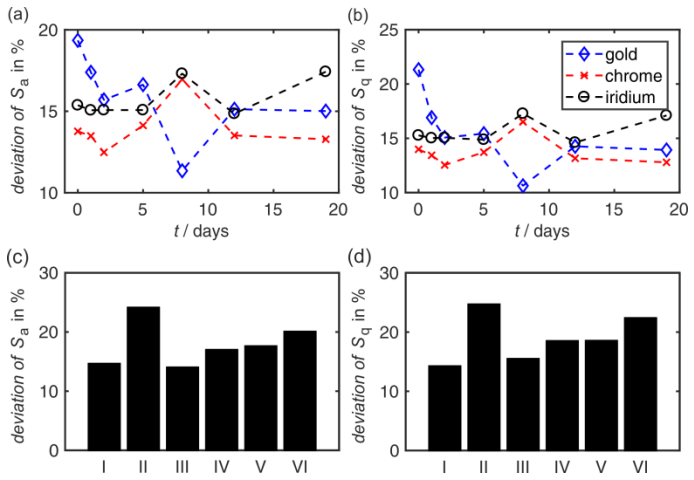

Fig. 12. Results of the type ARS material measure. (a)-(b): aging study; (c)-(d): scaling study. I-VI as described in Fig. 8.

Optics EXPRESS

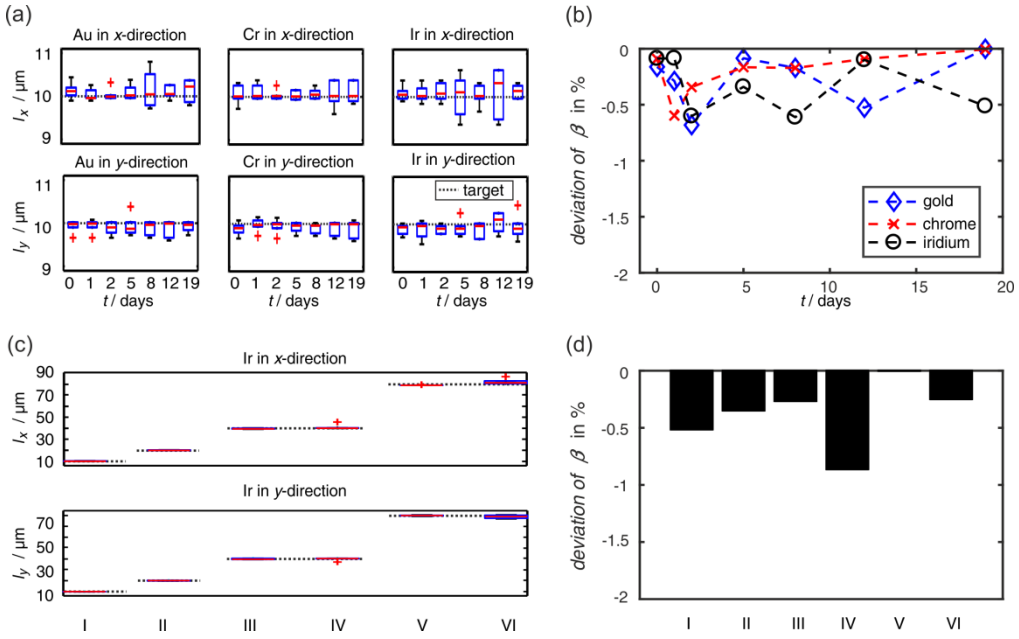

Fig. 13. Results of the type ACG material measure. (a)-(b): aging study. Pitch lengths l_x,l_y and deviation of the angle β between the x- and y-grating; (c)-(d): scaling study. I-VI as described in Fig. 8.

Funding

Deutsche Forschungsgemeinschaft (DFG), Collaborative Research Center 926.

Acknowledgments

The authors gratefully acknowledge financial support from Deutsche Forschungsgemeinschaft (DFG) within the Collaborative Research Center (SFB) 926 as well as the Nano Structuring Center (NSC) for technical and professional support concerning sputter-coating and SEM images.